Numerical Study on the Periodicity of Urban Heat Dome Flow

Yan Zhang[1, 2, 3], Yifan Fan[1, 2, 3*]

[1]College of Civil Engineering and Architecture, Zhejiang University, Hangzhou, China
[2]Center for Balance Architecture, Zhejiang University, Hangzhou, China
[3] International Research Center for Green Building and Low-Carbon City, International Campus, Zhejiang University, Haining, China

Abstract. Under calm conditions where the background synoptic wind is weak or absent, the difference between city and rural temperature allows natural convection to develop. The turbulent circulation is also referred as urban heat island circulation or urban heat dome flow. The coupling of buoyancy, inertia, and vertical stability induces a natural periodicity in the urban heat dome flow. The periodicity in urban heat dome flow is often neglected in previous urban heat dome flow research. In this article, a high-precision CFD numerical method is applied, and the city is treated as a homogeneous flat plate with a specific shape. First of all, the real atmosphere model (around 20 km in length scale) are established and validated with water tank experiments. Convergent inflows at lower level and divergent outflows at upper levels can be observed. Then, the instantaneous 3D flow field distribution is analyzed, and the periodicity of the upper outflow region (f_{out}) after reaching the quasi-steady state is determined. Finally, cases with different city diameters (D), regional heat flux (H_0), and ambient potential temperature gradients ($\partial\theta/\partial z$) are designed and solved. A quantitative description of periodicity (f_{out}) and its relationship to buoyancy (B_0), inertia (U_d) and vertical stability (N) is presented.

1 Introduction

The most noticeable feature of urbanisation is its rapid expansion in size, which significantly alters underlying surface properties [1]. Cities affect the wind environment [2], thermal environment [3], and pollutant dispersion [4], forming a unique local climate, known as the urban climate [5]. Under stable and calm background conditions, the airflow in the city is dominated by different scales of natural convection [6], and an urban heat dome flow forms at the city scale [7]. The urban heat dome flow, which is characterised by lower-level convergent inflow and upper-level divergent outflow, is widely believed to affect the urban environment, energy efficiency, and health of residents. Urban heat dome flow has been evaluated using field measurements [8], numerical simulations [9], and water/air tank experiments [10]. The periodicity in urban heat dome flow is often neglected in previous urban heat dome flow research. However, the periodicity of the urban heat dome flow profoundly affects the temperature field of the wind field inside the city, which in turn affects the diffusion of pollutants. The three-dimensional structure of the urban heat dome flow and the periodic changes of the flow field are shown in Fig. 1.

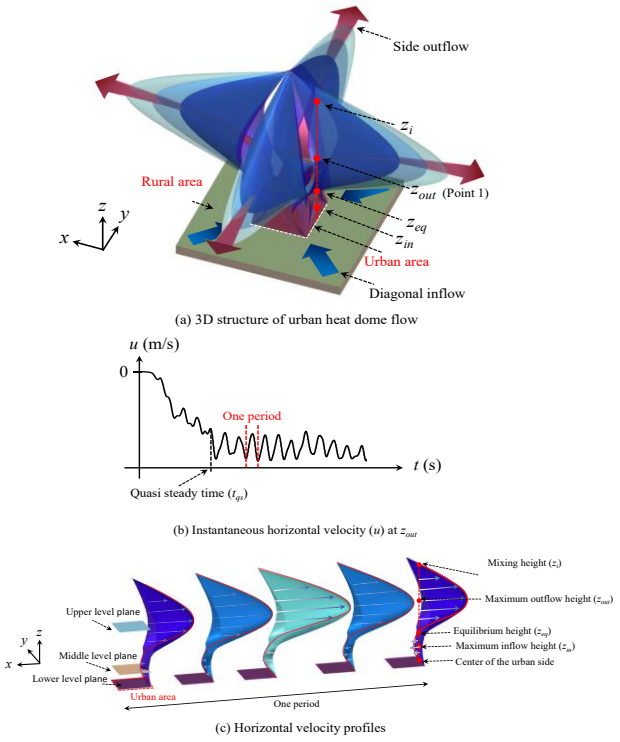

Fig. 1. The 3-D structure of the urban heat dome flow over a square urban area at quasi-steady state. (b) Instantaneous horizontal velocity (u) of the point 1 at z_{out}. (c) The 3D structure of the urban heat dome flow over a square urban area at quasi-steady state. (c) The deformation of Velocity profile at the side of city during one period.

Corresponding author: yifanfan@zju.edu.cn

2 Methods

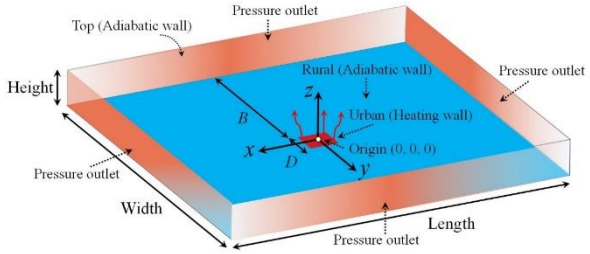

Fig. 2. The computational domain and boundary conditions for simulating 3D urban heat dome flow over a square urban area. The origin of coordinates is located in the centre of the urban; D and B are urban diameter and the distance from urban edge to domain boundary.

In this study, an ideal square city with uniform heating is considered (Fig. 2). In Fan's studies [11], a square heater with a diameter (D) of 0.12 m was placed at the middle of the water tank's bottom surface (0.4 × 0.4 × 0.5 m, length × width × height) to simulate an ideal square urban area. The flow was considered to have reached a quasi-steady state after 120 s of heating. Full-scale atmospheric cases (Case 1–4, in Table 1) were studied (the side length of the urban area was 20 km). The calculation domain was set to 100 × 100 × 2 km (length × width × height).

Table 1. Summary of all cases. buoyancy frequency N are presented for background temperature stratification. Heat flux H_0 and Froude number Fr are used to consider city area as an isolated heated surface. $u_D = g\beta H_0 D/\rho C_p$ is the convective velocity. g is the gravitational acceleration [m s^{-2}], ρ is density [kg m^{-3}], and C_p is the specific heat capacity of the fluid [J kg^{-1} K^{-1}], β is the thermal expansion coefficient [K^{-1}].

Case	D (km)	N (s^{-1})	H_0 (W m^{-2})	Fr	u_D (m s^{-1})	z_i (m)
Case 1	2×10^4	0.018	200	0.013	4.73	705
Case 2	2×10^3	0.018	100	0.048	1.74	230
Case 3	2×10^4	0.018	300	0.015	5.42	800
Case 4	2×10^4	0.026	200	0.009	4.73	608

The commercial software ANSYS Fluent (v17) (Ansys, Canonsburg, PA, USA) was used to solve the continuity, momentum, and energy equations. To ensure the proper settings of potential temperature and stable stratification were used, vertical coordinate transformation [12] was applied and a new set of governing equations was obtained, Eq. (1-3). All simulations were performed using transformed coordinates. After the simulation, the results were converted back to the Cartesian coordinate system with the physical height for better presentation and analysis. The hydrostatic, Boussinesq and anelastic assumptions are approximations are used for simplifying the momentum equation and the governing equations of continuity, momentum, and energy were rewritten as Eq. (1-3):

$$\nabla \cdot \vec{V} = 0 \tag{1}$$

$$\frac{d(\rho_0 \vec{V})}{dt} = -\nabla p + \mu \nabla \vec{V}^2 + \rho_0 \beta (T - T_0) g + \vec{F_n} = 0 \tag{2}$$

$$\frac{d(\rho_0 C_p T)}{dt} = \nabla (k \nabla T) + S_T \tag{3}$$

where t is time [s], μ is the molecular viscosity for the friction term [kg m^{-1} s^{-2}], and k is the incompressible conductivity [W m^{-1} K^{-1}]. The Boussinesq assumption was used in the momentum equation (Eq. 2) and the coordinate transformed term ($\vec{F_n}$) were included in Eq. (4) and the parameters z_n, w_n, J and ξ were defined as Eq. (5-8) to simplify the equation:

$$\vec{F_n} = \begin{bmatrix} 0 \\ 0 \\ (J^2 - 1)\rho_0 \beta (\theta - T_0) g + \xi \rho_0 {w_n}^2 J - p_n \xi (J + 1 + \xi z_n) \end{bmatrix} \tag{4}$$

$$z = -\frac{1}{\xi} ln(1 - \xi z_n) \tag{5}$$

$$w = \frac{\rho_0}{\rho_s} w_n = e^{\xi z} w_n \tag{6}$$

$$J = 1/(1 - \xi z_n) \tag{7}$$

$$\xi = -\frac{1}{z} \left(\frac{g}{R\Gamma} - 1\right) ln\left(\frac{T_0 - \Gamma z}{T_0}\right) \tag{8}$$

The results of water tank experiments conducted by Fan et al. [11] were used to validate the numerical model. A vertical profile of the horizontal velocity (u) was extracted at the centre of the city edge (x/D = 0.5, y/D = 0). The dimensionless horizontal velocity $U_W{}^*$ ($U_W{}^* = u/u_D$, where subscript 'W' represents the water tank) was introduced.

As suggested by Fan [13], the non-dimensional horizontal velocity profiles in reduced-scale water tank models and real atmospheric scale models should be corrected using the Prandtl number (Pr) for comparison. According to a previous study [13], Eq. (9) was used for the correction:

$$U_W{}^* = U_A{}^* \left(\frac{\mathrm{Pr_W}}{\mathrm{Pr_A}}\right)^{-c} \tag{9}$$

where $\mathrm{Pr_W}$ and $\mathrm{Pr_A}$ are the Prandtl numbers for water and air, respectively, and $U_W{}^*$ and $U_A{}^*$ are the time-mean horizontal velocity scales used for water and air, respectively. The $\mathrm{Pr_W}/\mathrm{Pr_A}$ and c were set to 8.75 and 0.48, respectively. In Fig. 3., the velocity distribution of case 1 with 8.36 million grids fits well with the experiment, while the results of the real atmospheric scale model successfully predicted the inflow at the lower level (z/z_i=0.2) and the strong outflow at the upper level (z/z_i=0.8).

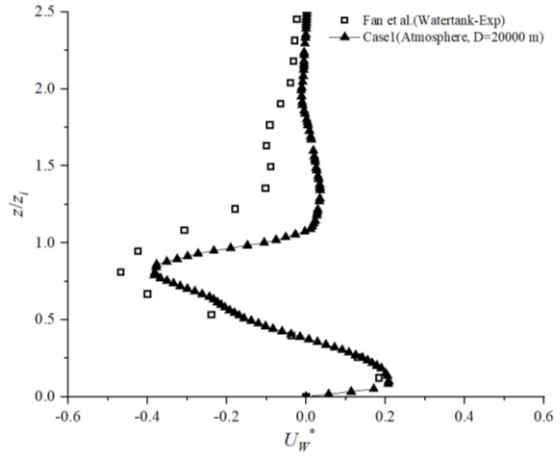

Fig. 3. The average horizontal velocity component vertical profiles at the urban edge ($x/D = 0.5$, $y/D = 0$, solution time from 10,000 s to 15,000 s for full-scale atmosphere model). Data for the water tank experiments were obtained from Fan et al. [11].

3 Results

3.1 The velocity and temperature field

Based on the vertical distribution profile of the mean horizontal velocity u at the urban edge ($x/D = 0.5$, $y/D = 0$), the maximum inflow height (z_{in}), equilibrium height (z_{eq}), and maximum outflow height (z_{out}) could be determined (Fig. 1). For case 1, the velocity and temperature fields on the horizontal planes at different heights were obtained, as shown in Fig. 4. U and T represent the time-averaged velocity and temperature (from 10,000 s to 15,000 s in the quasi-steady state).

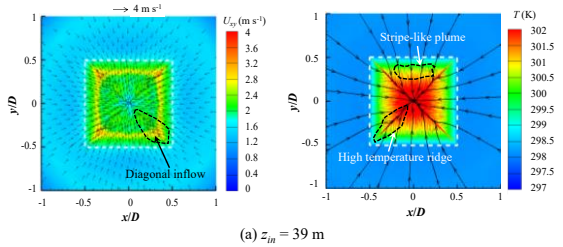

(a) z_{in} = 39 m

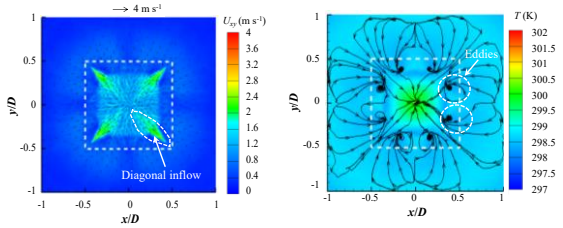

(b) z_{eq} = 250 m

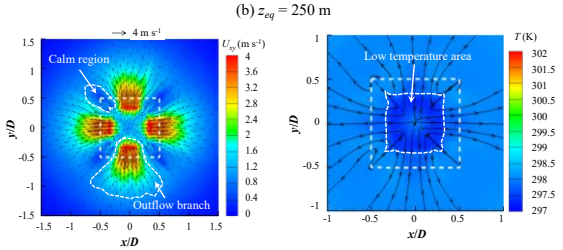

(c) z_{out} = 472 m

Fig. 4. The mean velocity fields ($U_{xy} = \sqrt{U_x{}^2 + U_y{}^2}$, U_x and U_y are the time averages of u and v) on different horizontal planes at quasi-steady state for Case1 (in left). Streamlines and the distribution of the real temperature for Case1 (in right). The dashed white squares denote the location of the urban area.

At the maximum inflow height (z_{in}), the flow field presented a standard convergent inflow along the diagonals, as shown in Fig. 4(a) left. The maximum horizontal inflow speed (U_{xy}) at z_{in} = 39 m was approximately 3 m s^{-1}. The temperature fields are shown in right. The solid black lines represent the streamlines of flow, the arrows represent the direction of velocity. At the lower level, the temperature in the central area of the city exceeded 301 K, which is approximately 3 K higher than that in the edge area. Stripe-like thermal plumes were observed in the edge regions, which were also observed in the water tank experiments [14]. Simultaneously, high-temperature ridges were observed near the diagonal lines. At the intermediate level (Fig. 4b), the inflow weakens, and the outflow begins to appear. The high-speed area (greater than 3m s^{-1}) inside the city was greatly reduced at z_{eq} = 250 m. Diagonal inflows remained, and the speed on the diagonals was higher than that in other areas. The high-temperature area shrank towards the city centre, and its temperature was approximately 200 K. Two symmetrical large eddy structures appear at each edge of the square city. For the upper level (Fig. 4c), the four side areas exhibited obvious divergent outflows. Four low-pressure and low-speed recirculation regions (calm regions) formed between each of the two high-speed outflow branches. The real temperature was lower in the urban area than in the rural area, caused by the overshoot effect of the urban heat dome flow.

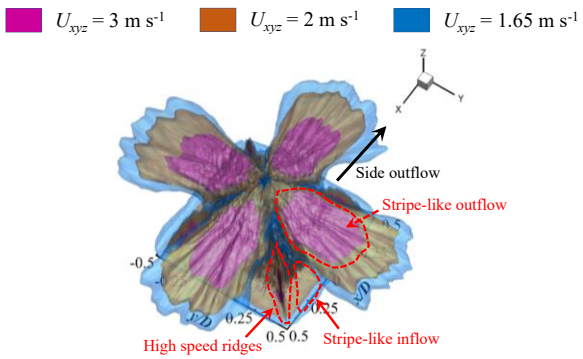

(a) Velocity iso-surface distribution

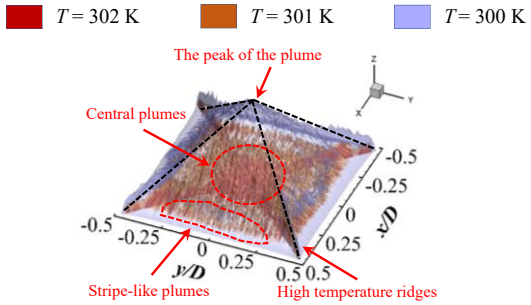

(b) Temperature iso-surface distribution

Fig. 5. 3D urban heat dome flow structure of case1 visualized by iso-surface of average velocity U_{xyz} and temperature ($U_{xyz} = \sqrt{U_x{}^2 + U_y{}^2 + U_z{}^2}$, where Ux, Uy, and Uz are the time averages of u, v and w, respectively, with solution times from 10,000 to 15,000 s).

The 3D isosurfaces of the velocity and temperature are shown in Fig. 5. In Fig. 5(a), an iso-surface of 3m s^{-1} was observed along the diagonal at the lower level. As the height increases, the iso-surface of 2 m s^{-1} gradually shrank and was close to the diagonal, resulting in a high-speed ridge form. The isosurface in the side region presented a stripe-like inflow formed by the disturbance of sub city-scale thermal plumes. At the upper level, the outflows above the four sides of the city presented a four-leaf clover structure, which is consistent with the water tank experiments conducted by Fan et al. [14]. Stripe-like outflows were also observed at this level. The 3D iso-surface distribution of temperature is shown in Fig. 5(b). Stripe-like thermal plumes were observed in the urban edge regions and high-temperature ridges near the diagonal lines. Many high-temperature plumes were gathered in the central urban area.

3.2 The periodicity of urban heat dome flows

The velocity profiles at the city side were extracted and Fourier transform was performed on the instantaneous velocity signal at point 1 (z=z_{out}), as shown in Fig 6. The frequency f_{out} corresponding to the magnitude peak was obtained then. f_{out} is the reciprocal of the period, which can reflect the periodicity of the flow. Large f_{out} values correspond to short periods.

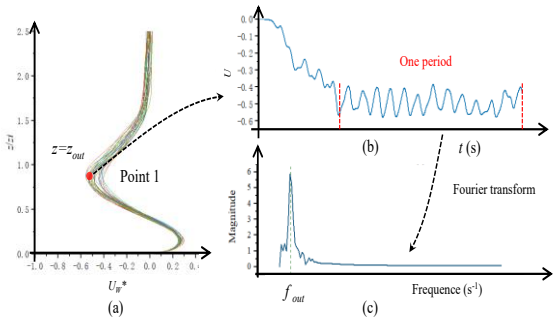

Fig. 6. (a) Instantaneous dimensionless velocity (U_W*) profile distribution at the city edge. (b) The original instantaneous dimensionless velocity U at point 1. (c) Calculated magnitude diagram after Fourier transform to show the frequency f_{out} corresponding to the peak.

The periodicity of the urban heat dome flow is evaluated by f_{out}, which is related to buoyancy, inertia, and vertical stability. As in Eq.(10), a formula for calculating f_{out} is attempted to be derived.

$$f_{out} = {B_0}^{0.65} \times {u_D}^{-1.3} \times N^{0.35} \quad (10)$$

$$B_0 = {g\beta H_0}/{\rho C_P} \quad (11)$$

$$N = [-(g/\rho_0)\frac{\partial \rho}{\partial z}]^{1/2} \quad (12)$$

where ρ_0 is the reference density [kg m^{-3}].

Finally, case2-4 with different city diameters (D), regional heat flux (H_0), and ambient potential temperature gradients ($\partial\theta/\partial z$) are designed and solved. The values of f_{out} corresponding to cases 1-4 are shown in Fig. 7. It can be found that the decrease of the city diameter and the increase of the heat flux density and temperature gradient lead to the decrease of the outflow frequency and the increase of the outflow period. The results calculated by Eq. 10 are in good agreement with those obtained from the simulation.

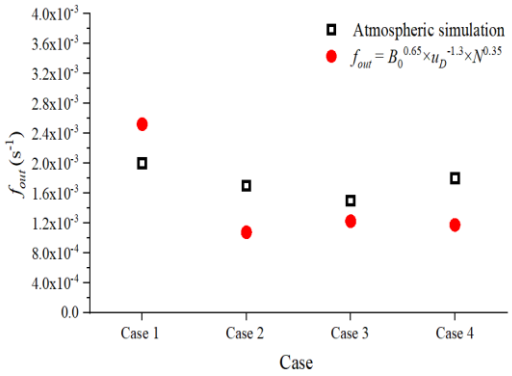

Fig. 7. Diagram of frequency f_{out} for different cases. The black hollow squares are numerically calculated values, and the red solid circles represent the formula-fitted values.

4 Conclusion

(1) The CFD method was applied to an urban heat dome flow simulation for mesoscale atmospheric cases. Convergent inflows at lower level and divergent outflows at upper levels can be observed.

(2) The periodicity of the upper outflow region ($f_{out} = {B_0}^{0.65} \times {u_D}^{-1.3} \times N^{0.35}$) after reaching the quasi-steady state is determined. The results calculated by the formula are in good agreement with those obtained by the simulation.

(3) The decrease of the city diameter, the increase of the heat flux density and the increase of the temperature gradient all lead to the decrease of the outflow frequency and the increase of the outflow period.

References

1. Y. Ashie, T. Kono, INT J CLIMATOL, 31, 174-188 (2011)
2. Y. Tominaga, J VISUAL, **15**, 269-276 (2012)
3. H. Tao, J. Xing, G. Pan, P. Jonathan, L. Ran, S. Wang, X. Chang, G. Li, F. Chen, J. Li, FRONT ENV SCI ENG, **16**, 44 (2022)
4. S. R. Hanna, O. R. Hansen, M. Ichard, D. Strimaitis, Atmos Environ, **43**, 262-270 (2009)
5. G. Y. Ren, Advances in Climate Change Research, **6**,1-6 (2015)
6. Y. Zhao, L. W. Chew, A. Kubilay, J. Carmeliet, Build Environ, **184**, 107163 (2020)
7. Y. Fan, J. C. R. Hunt, Y. Li, J Environ Sci, **59**, 63-71 (2017)
8. J. H. Shreffler, J APPL METEOROL, 18, 1512-1520 (1979)
9. A. Lemonsu, V. Masson, Boundary Layer Meteorol, 104, 463-490 (2002)
10. J. Hidalgo, G. Pigeon, V. Masson, METEOROL ATMOS PHYS, 102, 243-262 (2008)
11. Y. Fan, J. Hunt, S. Yin, Y. Li, Theor. Appl. Climatol., 1-15 (2018)
12. X. Wang, Y. Li, Build Environ, **99**, 82-97 (2016)
13. Y. Fan, Y. Li, X. Wang, F. Catalano, JAMC, **55**, 2151-2164 (2016)
14. Y. Fan, Y. Li, Q. Wang, S. Yin, Int. J. Heat Mass Transf., 140, 660-670 (2019)